Biosensors and Bioelectronics 33 (2012) 82–87

Contents lists available at SciVerse ScienceDirect

Biosensors and Bioelectronics

journal homepage: www.elsevier.com/locate/bios

Femtosecond laser nanostructuring for femtosensitive DNA detection

M. Alubaidy[a], L. Soleymani[c,d], K. Venkatakrishnan[a], B. Tan[b,*]

[a] Department of Mechanical Engineering, Ryerson University, 350 Victoria Street, Toronto, Ontario, Canada M3N 2H8
[b] Department of Aerospace Engineering, Ryerson University, 350 Victoria Street, Toronto, Ontario, Canada M3N 2H8
[c] Department of Engineering Physics, McMaster University, 1280 Main Street West, Hamilton Ontario, Canada L8S 4L7
[d] School of Biomedical Engineering, McMaster University, 1280 Main Street West, Hamilton Ontario, Canada L8S 4L7

ARTICLE INFO

Article history:
Received 14 October 2011
Received in revised form
30 November 2011
Accepted 14 December 2011
Available online 23 December 2011

Keywords:
Nanofibers
DNA
Biosensor
Ultrafast laser

ABSTRACT

In this paper, a new concept to achieve improved probe–target recognition has been devised by introducing a novel class of DNA-functionalized three-dimensional (3D), stand-free, and nanostructured electrodes. The gold nanofibrous electrodes were created using MHZ ultrafast laser material processing in air at ambient conditions. The developed nanofibrous DNA biosensor was characterized by cyclic voltammetry with the use of ferrocyanide as an electrochemical redox indicator. Currently, electrochemical signal enhancement which is of great significance for improving the sensitivity in DNA detection remains a great challenge. Through, enhanced surface area-to-volume ratio and more efficient arrangement of probe molecules on nanofibrous electrodes, our newly developed electrode system overcomes some of the sensitivity challenges of the existing systems. This nanofiber-based system realizes femtomolar (fM) sensitivity toward complementary target DNA, and demonstrates a very wide dynamic range (from 1 fM to 1 nM).

1. Introduction

DNA is the hereditary material within the cellular chromosomes, and its sequence significantly influences human health (Soleymani et al., 2009). Genetic code is inherited through the sequence of DNA bases, and variations in DNA sequence can be indicative of disease development. (Wong and Gooding, 2005; Wong and Melosh, 2010). DNA sequence detection has received increased attention due to its potential applications in many fields including biomedical engineering, clinical diagnosis, and environmental protection (Duggan et al., 1999; Fang et al., 1999). Capture and subsequent detection of DNA sequences through hybridization with complementary probe DNA is the underlying principle of many existing DNA biosensors and is of significant interest. In previous reports, the surface of a sensor is modified with nucleic acids probes capable of generating an optical (Rong et al., 2008; Wang et al., 2006), gravimetric (Mannelli et al., 2005), piezoelectric (Su et al., 2003), electrical or electrochemical (Chen et al., 2007; Zeglis and Barton, 2007) signal upon hybridization with a complementary sequence (Kirk et al., 2002; Baudhuin et al., 1989). Accordingly, the detection sensitivity of DNA biosensors is determined by the signal variation resulting from hybridization events, hence the significance of signal enhancement for improving the DNA detection sensitivity. Electrochemical techniques for DNA detection offer several advantages in comparison with the other existing techniques. These techniques are simple, rapid, low-cost and highly sensitive (Drummond et al., 2003; Liu et al., 2008; Li et al., 2010). Electrochemical DNA detection with high sensitivity can be achieved by substrate nanostructuring aiming at increasing the amount of immobilized DNA probe molecules and improving the recognition properties of immobilized DNA probes (Hill et al., 2009; Liu et al., 2010). Many efforts have been devoted to enhancing the hybridization signal of DNA biosensors (Jin et al., 2001, 2003; Sun and Xia, 2002), however, a low-cost, simple and scalable strategy for signal amplification remains a challenge (Fang et al., 2009).

Nanomaterials have received increasing attention due to their unique physical and chemical properties caused by their quantum confinement, high surface area to volume ratio, and macro quantum tunnel effects (Li et al., 2007; Yamada et al., 2003; Zhao et al., 2007; Jena and Raj, 2007); and various nanomaterials such as nanoparticles, nanowires, nanotubes, and nanospheres, have been prepared (Willner and Katz, 2007; Xia et al., 2008; Wang et al., 2003). The enhanced performance of nanomaterial-based devices provides a new opportunity for amplifying DNA hybridization signals through coupling DNA with such materials. Gold nanoparticles provide a stable immobilization substrate for biomolecules as it helps retain their bioactivity.

Nanostructured gold electrodes could be constructed by various strategies including direct electrostatic assembly, covalent linking (Delvaux et al., 2003), polymer entrapment or co-mixing,

* Corresponding author. Tel.: +1 4169795000x4879.
E-mail address: tanbo@ryerson.ca (B. Tan).

0956-5663/$ – see front matter © 2012 Elsevier B.V. All rights reserved.
doi:10.1016/j.bios.2011.12.023

sol–gel processes (Lin et al., 2004), electrochemical etching, and electrodeposition (Li and Shi, 2005). Even though the development of gold nanostructures by electrodeposition method has been widely used for the applications in biosensor, it still requires the use of catalyst and it involves a lot of complicated steps (Vītiņa et al., 2011). We reported a unique method for nanoparticles generation using femtosecond laser material processing at ambient conditions. The fibrous structure generation is explained by nucleation and condensation of plasma plume generated during the irradiation process. Bulk quantity of nanoparticles agglomerate by fusion, and form interweaving three dimensional fibrous structures that show certain degree of assembly (Tan and Venkatakrishnan, 2009). Unlike conventional methods, the new technique is capable of nanostructuring under ambient conditions without using any catalyst. It is a single-step technique and the precursors are common materials. Also, the new technique generates intact weblike nanostructures with the ability to control the size of the nanostructures by properly adjusting the laser parameters.

In this work, we devise a new concept to achieve improved probe–target recognition by introducing a novel class of DNA-functionalized nanofibrous electrodes. An ultrafast laser is used to prepare 3D gold nanofibrous electrodes that allow ultrasensitive, and label-free discrimination of complementary and non-complementary DNA analytes. The 3D weblike nanofibrous structure significantly influences the sensitivity of the nucleic acid assay and it is essential for the performance of the nano/microelectrodes as ultrasensitive electrochemical detectors. It is also highly beneficial for biosensing applications because of the increased effective surface area.

2. Experimental

The laser source used is a direct-diode pumped Yb-doped fiber oscillator/amplifier system capable of delivering a maximum of 15 W average power with a pulse repetition rate ranging from 200 kHz to 25 MHz and a wavelength of 1030 nm. The beam profile is Gaussian and the spot diameter is 10 μm. The samples (or working electrodes) used were 20 mm × 5 mm gold-coated (thickness of 350 nm) silicon wafers of 500 μm thickness. The laser beam is focused on the sample surface with a lens of focal length of 71 mm and scanned using a computer-controlled galvanometer. A computer controls the laser beam to irradiate the sample surface. A polarizer and analyzer are used to rotate and analyze the beam polarization. An acoustic modulator is used for pulse number control. The experiments were carried out in air at atmospheric pressure. The radiation fluence used was 0.5 J/cm^2 at a pulse repetition rate of 25 MHz with an interaction time of 1 ms and with the pulse width of 214 fs. Two sets of samples were prepared with same experimental conditions. One set was used to generate nanofibrous structures inside a 5 mm × 5 mm area of the Au/Si wafer. The second set was used to generate a 5 mm × 5 mm on the Au/Si wafer to guarantee the same dimensions of the first set but with bare gold on the surface. The rest of the wafer was insulated in both sets with insulating material (Ormocore) except for a 2 mm × 5 mm area on the opposite side of the laser treated area to allow for electrical connection.

The synthetic oligonucleotides were purchased from Integrated DNA Technologies, Inc. (USA). Their base sequences are: probe DNA: 5-/5ThioMC6-D/ATA AGG CTT CCT GCC GCG CT-3, complementary target DNA: 5-AGC GCG GCA GGA AGC CTT AT-3 and non-complementary target DNA: 5-TTT TTT TTT TTT TTT TTT TT-3. Cyclic voltammetry (CV) measurements were performed with a PalmSense electrochemical sensor (USA). All electrochemical experiments were performed with a conventional three-electrode system. The reference and auxiliary electrodes were purchased from BASi (USA). We used a platinum wire auxiliary electrode, an Ag/AgCl reference electrode, and home-built nanofibrous and unprocessed gold working electrodes.

Fig. 1 shows a schematic representation of the fabrication procedure of the DNA biosensor. The immobilization of thiolated probe DNA was performed by the deposition of a 100 μL solution containing 5 μM single stranded thiolated DNA, 20 mM $MgCl_2$, 25 mM sodium chloride and 25 mM phosphate buffer on the planar and nanofibrous modified gold electrodes for 1 h in a dark humidity chamber at room temperature.

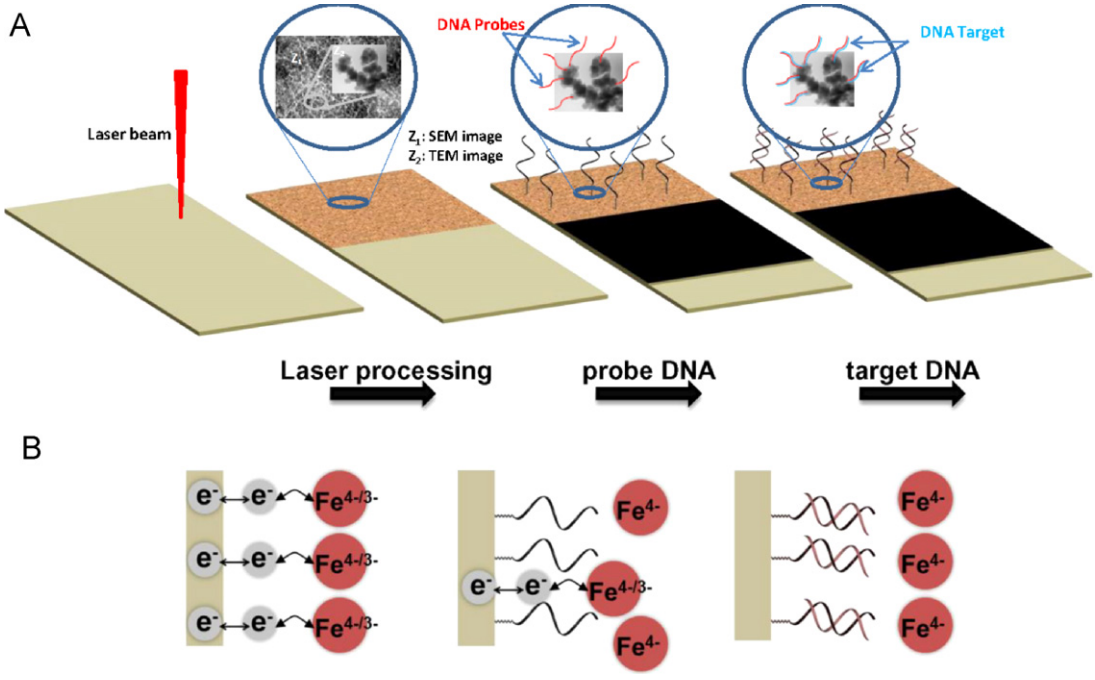

Fig. 1. Schematic representation of electrochemical DNA detection using gold nanofibrous electrodes (GNE) (A). Steps involved in fabricating single stranded DNA-modified GNEs (B). Label-free electrochemical detection using the redox reporter potassium ferrocyanide (Fe^{4-}).

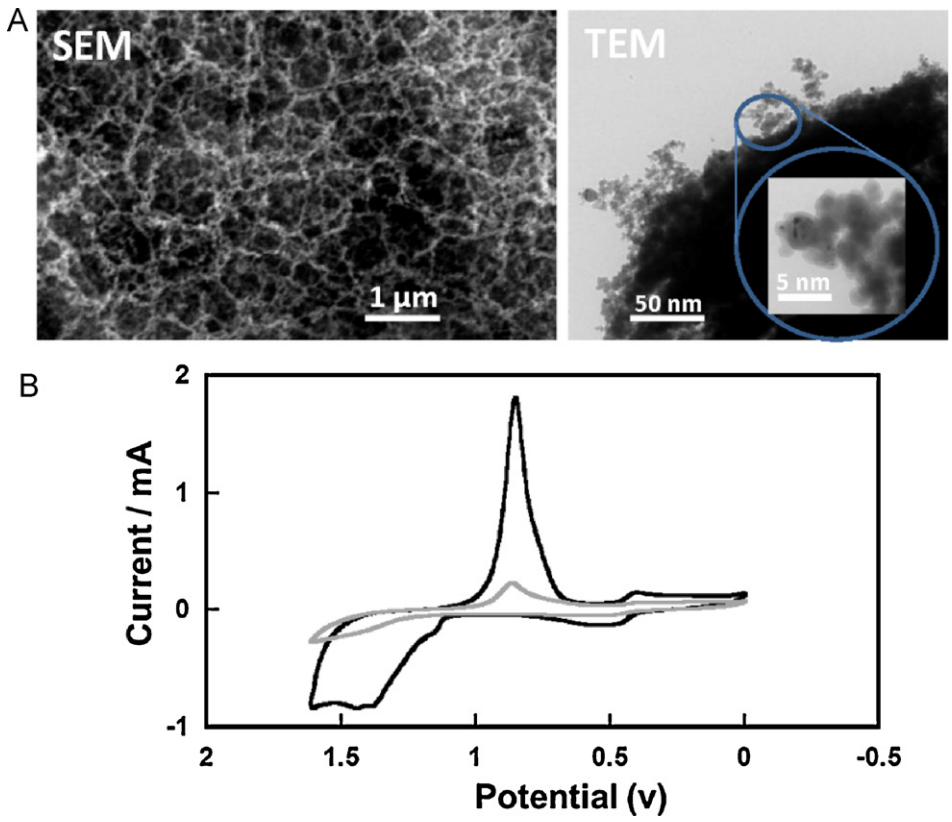

Fig. 2. Characterization of GNEs. (A) Scanning electron microscopy and transmission electron microscopy images of gold nanofibers. (B) Cyclic voltammogram in H_2SO_4 of gold electrode before (gray) and after laser processing and creation of gold nanofibers.

Then, the electrodes are washed after probe deposition for 10 min using 25 mM sodium chloride (NaCl) and 25 mM phosphate buffer pH 7 solution (25/25). Probe-modified electrodes are scanned in and 2 mM $Fe(CN)_6^{3-}$. Following the first electrochemical readout and washing the electrodes with an aqueous solution of 25 mM sodium chloride and 25 mM phosphate buffer, the two electrode (planar and nanofibrous) are incubated in a dark humidity chamber with different concentrations of non-complementary DNA targets in 25 mM sodium chloride (NaCl) and 25 mM phosphate buffer pH 7 solution (25/25) at 37 °C for 1 h. Probe-modified electrodes are scanned again in 2 mM $Fe(CN)_6^{3-}$ and the process is repeated for the complementary and non complementary DNA targets. To determine whether any of the on-electrode probe sequences are successfully hybridized, the reductive catalytic current is measured after hybridization. The change in peak reductive current is documented for different probe/target combinations.

3. Results and discussion

3.1. Nanoelectrodes generation

SEM micrographs of the working electrode surfaces around the laser-irradiated spots are shown in Fig. 2(a). Weblike fibrous nanoparticle aggregates with certain degree of porosity are observed in and around the laser-irradiated spots. This was consistently observed in all of the samples processed, under different conditions, during this series of experiments. Fig. 2(a) also demonstrates the TEM analysis of the generated nanofibrous structure. The size of Au nanofibers in the fibrous nanoparticles aggregate structure is as small as 2 nm as evident from TEM analysis. The relative surface area of the nanofibrous and unprocessed electrodes was evaluated by comparing the amount of charge involved in the reduction of gold oxide under acidic conditions. (José et al., 2000) Fig. 2(b) demonstrates the cyclic voltammogram of processed and unprocessed electrodes in 0.5 M H_2SO_4. According to this figure, the effective surface area of nanofibrous modified electrode is about 10 times larger than the area of the planar gold electrode. Whereas, the surface area increase for the common gold nanoparticles electrodeposited electrode is only about 2–4 times compared with that of planar gold electrode (Liu et al., 2010). This further indicated that the three-dimensional porous nanostructures created by laser processing largely increased the effective electrode surface area.

Processing of materials using femtosecond laser radiation involves steps such as non-linear absorption, plasma formation, shock wave propagation, melt propagation, and resolidification. Laser radiation energy is absorbed by the electrons in materials through multiphoton and avalanche ionization and then transferred to the lattice within few picoseconds, after which heat diffusion into material begins. At the same time, the ionized material is removed from the surface through ablation in the form of expanding high pressure plasma. A smaller portion of the absorbed energy from laser radiation remains in the material as thermal energy.

The melt time and the pulse repetition rate have significant influence on the growth of nanofibers. The lifetime of the molten material is determined by the time in which the energy diffuses into the substrate. The estimated melt time based on one-dimensional heat conduction model for gold is about 0.6 μs, which is longer than the pulse separation time of 0.125 μs used in the present experiment. As a result, resolidification of molten material throughout the irradiation process is avoided. This helps for the continuous growth of the nanofibers with successive laser pulses and only resolidified particles are observed on the irradiated surface as shown in Fig. 3. The forces acting on the molten material are interacting capillary forces coupled with thermal processes (Marangoni force) (Tan and Venkatakrishnan, 2009) and hydrodynamic forces

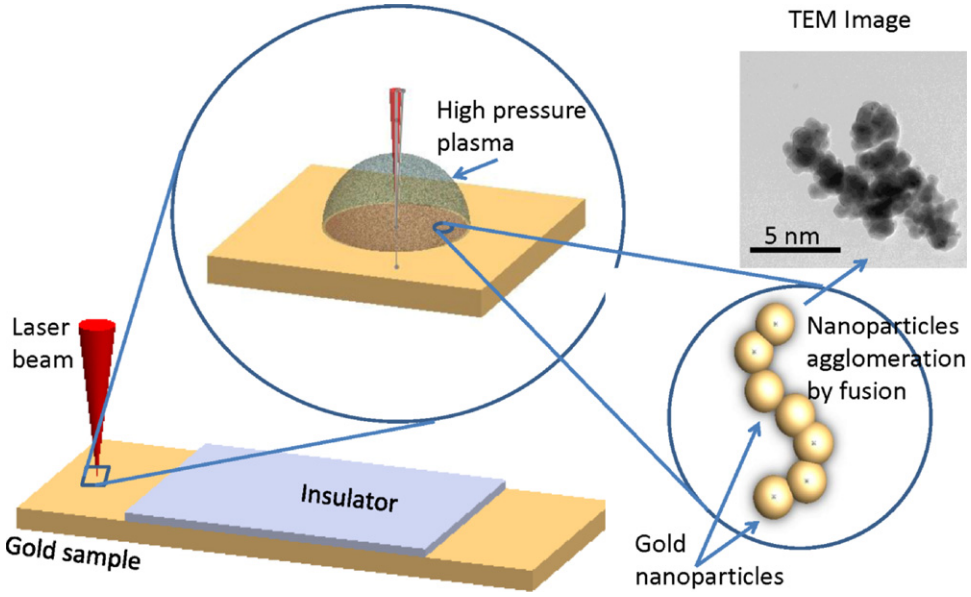

Fig. 3. Ionized material is removed from the surface through ablation in the form of expanding high pressure plasma and the nanoparticles agglomerate by fusion to form nanofibers.

exerted by the plasma above the surface (Ivanov et al., 2008). The temperature gradient on the molten surface, which follows the Gaussian intensity profile of the laser beam induces the thermo-capillary flow (Vorobyev and Guo, 2006). The temperature gradient in turn creates surface tension gradient that drives material from the hot center to the cold periphery. The nanofibers are grown along and perpendicular to the substrate surface. The growth of nanofibers can be explained by the strong temperature gradients produced by the tightly focused femtosecond laser pulses which cause acceleration of the molten liquid at the melt/air interface. This acceleration as well as the plasma plume induces a pressure gradient from the center toward the periphery in the molten liquid of the laser-drilled microvias. The highly energetic droplets that are formed inside the molten material are moved to the exterior of the laser-drilled microvias due to pressure gradient in the molten liquid and provide the heads of nanojets which eventually draws the nanofiber from the melt and because of shorter duration of the laser pulse the fibers drawn are immediately solidified.

The nanofibers and nanoparticles in the generated 3D nanostructures are attractive probe candidates because of their small size (1–100 nm) and correspondingly large surface-to-volume ratio, target binding properties, and overall structural robustness. The actual structure apparently resembles a lattice of tightly packed branches and sub-branches of gold nanoparticles leaving 3D stand free nanostructures that have weblike appearance. Each nanoparticle in this nanostructure would be the base for a nanoprobe. This result in a significant increase of the effective number of nanoprobes compared to the conventional 2D gold nanostructures. The size of a nanomaterial can be a crucial factor because a target binding event involving the nanomaterial can have a significant effect on its physical and chemical properties; therefore the generated 3D nanofibrous structures by ultrafast laser would provide an enhanced mode of signal transduction than other kind of structures made of the same material.

3.2. Biosensor sensitivity

Fig. 4(a) shows the cyclic voltammograms obtained for the modified electrodes in 1 mM $Fe(CN)_6^{4-}$ solution at the scan rate of 100 mV/s. A pair of redox peaks was observed on the nanofibrous modified electrode with the anodic (E_{pa}) and cathodic (E_{pc}) peak

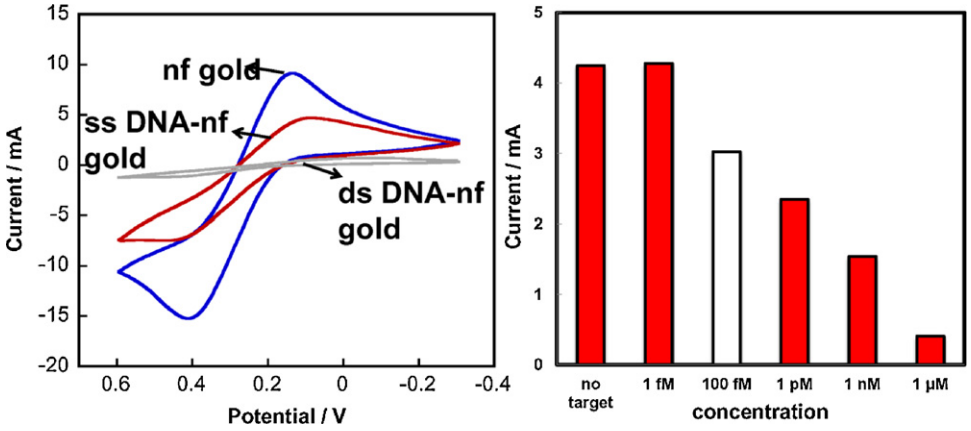

Fig. 4. Detection of DNA hybridization using GNEs (A). Cyclic voltammogram in 2 mM potassium ferrocyanide nanofibrous gold, ssDNA modified nanofibrous gold, and dsDNA modified nanofibrous gold (B). Detection limit of the GNEs. The reduction current measured at 0.15 V is plotted for increasing concentrations of complementary DNA targets hybridized at 37 °C for 60 min. The lowest concentration that a detectible current decrease is measured is shown with a white bar.

potential of 0.08 V and 0.42 V, respectively. After probe DNA immobilization on the nanofibrous modified electrode, the peak current of $Fe(CN)_6^{3-/4-}$ was largely inhibited and the peak to peak potential separation ($\Delta E_{p)}$ was largely increased. This could be explained by electrostatic repulsion of $Fe(CN)_6^{3-/4-}$ from the negatively charged DNA film. This behavior is line with results described in literature in immobilization of DNA on gold macroelectrodes (Lapierre et al., 2003). A further decreased peak current and increased ΔE_p was observed after hybridization of probe DNA with target complementary DNA. This could be well assigned that the introduction of complementary DNA increases the negative charge responsible for the increased repellence of redox species. The same experiment was done with the non-complementary DNA. However, there is no significant decrease in the voltammetric signals of non-complementary compared to the complementary DNA and also these signals are close to the ssDNA probe signal.

To evaluate the performance of nanofibrous modified electrode, the peak current change before and after hybridization of probe DNA with complementary target DNA was further studied. The peak current of $Fe(CN)_6^{3-/4-}$ on the nanofibrous electrode decreases with the increasing target DNA concentration ranged from 1 fM to 1 μM as shown in Fig. 4(b). The peak current change of fabricated DNA sensor exhibited a linear correlation to the logarithm of the target DNA concentration ranged from 1 fM to 1 μM as shown in Fig. 4(b). The obtained low detection limit between 1 and 100 fM is among the lowest label-free and single step methods reported to date (Li et al., 2011).

In order to demonstrate that the enhanced detection limit of the gold nanofibrous electrode is indeed related to its unique structure, we compared its performance to an unprocessed gold electrode of the same geometric area. The peak reduction current of the ferrocyanide reporter at the gold nanofibrous electrode is larger than the unprocessed electrode as shown in Fig. 5. This is expected due to the enhanced surface area of the nanofibers as demonstrated in Fig. 4. The more striking result is that in addition to the higher current, which can lead to a higher signal to noise ratio, there is a larger signal change when negatively charged DNA molecules interact with nanofibrous electrodes rather than unprocessed electrodes. This is true for both cases of deposition of DNA probes – 15% instead of 2% – and capture of DNA targets – 56% instead of 27%.

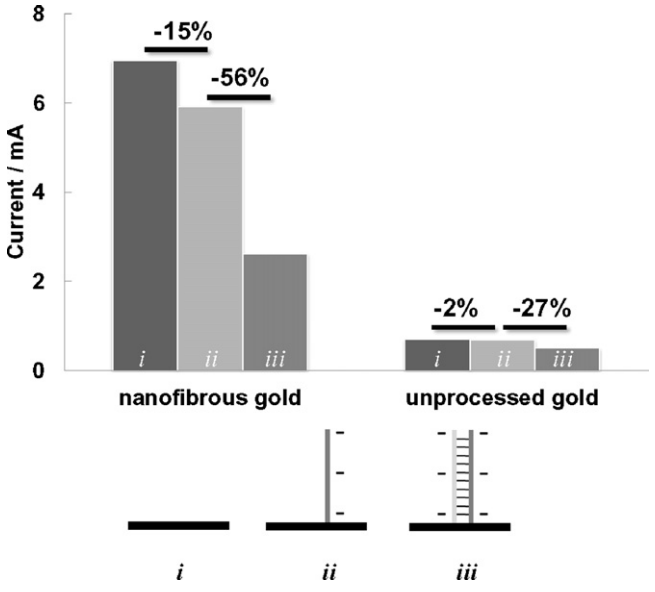

Fig. 5. Comparison of gold nanofibrous electrodes with unprocessed gold electrodes in detection of 100 fM complementary target. i, ii, iii represent the measurements performed on bare electrodes, ssDNA modified electrodes, And dsDNA modified electrodes respectively. All electrochemical currents represent the magnitude of the reduction peak of ferrocyanide at electrode. Percentages represent the changes in electrical current from stages i to ii and stages ii to iii.

The nanofibrous modified electrode with a huge surface area to volume ratio was considered to supply numerous attaching points for probe DNA immobilization. As well as, the immobilization orientation and assembly density of probe DNA may be well controlled by three-dimensional weblike structure of nanofibers for optimized hybridization efficiency. On the other hand, the hierarchical three-dimensional weblike structure in present case may diminish the repelling behavior when approaching of the target DNA toward the immobilized probe DNA and enhance the hybridization efficiency. The role of nanofibers in the sensitivity improvement can be explained by the small size of the generated nanofibers which could be as small as 2 nm and the weblike kind of nanofibrous structure which would increase number of probe DNA per unit area and hence, increase the probability of hybridization.

4. Conclusions

We constructed an electrochemical DNA biosensor based on 3D stand free nanofibrous electrodes for sensitive DNA sequence detection. The 3D nanofibrous structure was developed using MHz ultrafast laser in air and under ambient conditions. The nanofibrous structures largely increase the electrode surface area by about 10 times compared with that of bare gold electrode. The biosensor fabrication process was thoroughly investigated with cyclic voltammetry using $Fe(CN)_6^{3-/4-}$ as an electrochemical redox probe. The 3D gold nanostructure has a significant impact on increasing the immobilization amount of probe DNA and further hybridization amount with target DNA. The target DNA sequence could be quantified over the range from 1 fM to 1 nM. This nanofibrous biosensor could be used for the detection of target DNA in real biological and clinical samples and it could be further modified for applications in detection of cancers and infectious diseases.

References

Baudhuin, P., Van der Smissen, P., Beavois, S., Courtoy, J., 1989. Applications 2, 1–17.
Chen, C., Ko, F., Chen, C., Liu, T., Chang, E., Yang, Y., Yan, S., Chu, T., 2007. Appl. Phys. Lett. 91, 253103.
Delvaux, M., Demoustier-Champagne, S., Walcariusb, A., 2003. Electroanalysis 16, 190–198.
Drummond, T., Hill, M., Barton, J., 2003. Nat. Biotechnol. 21, 1192–1199.
Duggan, D., Bittner, M., Cheng, Y., Meltzer, P., Trent, J., 1999. Nat. Genet. 21 (supplement), 10–14.
Fang, X., Liu, X., Schuster, S., Tan, W., 1999. Am. Chem. Soc. 121, 2921–2922.
Fang, Z., Soleymani, L., Pampalakis, G., Yoshimoto, M., Squire, J., Taft, B., Sargent, E., Kelley, O., 2009. ACS Nano 3 (10), 3207–3213.
Hill, H., Millstone, J., Banholzer, M., Mirkin, C., 2009. ACS Nano 3, 418–424.
Ivanov, D., Rethfeld, B., O'Connor, G., Glynn, T., Volkov, A., Zhigilei, L., 2008. Appl. Phys. A 92, 791–796.
Jena, B., Raj, C., 2007. J. Phys. Chem. C 111, 6228–6232.
Jin, R., Cao, Y., Hao, E., Metraux, G., Schatz, G., Mirkin, C., 2003. Nature 425, 487.
Jin, R., Cao, Y., Mirkin, C., Kelly, K., Schatz, G., Zheng, J., 2001. Science 294, 1901.
José, M., Rodríguez, D., Melián, J., Peña, J., 2000. J. Chem. Educ. 77 (9), 1195.
Kirk, B., Feinsod, M., Favis, R., Kliman, R., Barany, F., 2002. Nucleic Acids Res. 30, 3295.
Lapierre, M., O'Keefe, M., Taft, B., Kelley, S., 2003. Anal. Chem. 75, 6327–6333.
Li, D., Yan, Y., Wieckowska, A., Willner, I., 2007. Chem. Commun. 34, 3544–3546.
Li, F., Han, X., Liu, S., 2011. Biosens. Bioelectron. 26 (5), 2619–2625.
Li, H., Sun, Z., Zhong, W., Hao, N., Xu, D., Chen, H., 2010. Anal. Chem. 82, 5477–5483.
Li, Y., Shi, G.Q., 2005. J. Phys. Chem. B 109, 23787–23793.
Lin, Y., Taylor, S., Li, H., Fernando, K., Qu, L., Wang, W., Gu, L., Zhou, B., Sun, Y., 2004. J. Mater. Chem. 14, 527–541.
Liu, G., Wan, Y., Gau, V., Zhang, J., Wang, L., Song, S., Fan, C., 2008. J. Am. Chem. Soc. 130, 6820–6825.
Liu, S., Liu, J., Han, X., Cui, Y., Wang, W., 2010. Biosens. Bioelectron. 25, 1640–1645.
Mannelli, I., Minunni, M., Tombelli, S., Wang, R., Spiriti, M., Mascini, M., 2005. Bioelectrochemistry 66, 129–138.
Rong, G., Ryckman, J., Mernaugh, R., Weiss, S., 2008. Appl. Phys. Lett. 93, 161109.
Soleymani, L., Fang, Z., Sargent, E.H., Kelley, S.O., 2009. Nat. Nanotechnol. 4 (12), 844–848.
Su, M., Li, S., Dravid, V., 2003. Appl. Phys. Lett. 82, 3562–3564.
Sun, Y., Xia, T., 2002. Science 298, 2176.

Tan, B., Venkatakrishnan, K., 2009. Opt. Express 17 (2), 1064–1069.
Vītiņa, I., Krūmiņa, A., Lubāne, M., Belmane, V., 2011. Mater. Sci. Eng. 23, 012024.
Vorobyev, A., Guo, C., 2006. Opt. Express 14, 2164–2169.
Wang, J., Liu, G., Merkoci, A., 2003. J. Am. Chem. Soc. 125, 3214–3215.
Wang, X., Cooper, K., Wang, A., Xu, J., Wang, Z., Zhang, Y., Tu, Z., 2006. Appl. Phys. Lett. 89, 163901.
Willner, I., Katz, E., 2007. Bioelectrochemistry 70, 2–11.
Wong, E., Gooding, J., 2005. Langmuir 21, 6957–6965.
Wong, I., Melosh, N., 2010. Biophys. J. 98, 2954–2963.
Xia, Q., Chen, X., Liu, J., 2008. Biophys. Chem. 136, 101–107.
Yamada, M., Tadera, T., Kubo, K., 2003. J. Phys. Chem. B 107, 3703–3711.
Zeglis, B., Barton, J., 2007. Nat. Protoc. 2, 357–371.
Zhao, L., Siu, A., Petrus, J., He, Z., Leung, K., 2007. J. Am. Chem. Soc. 129, 5730–5734.